Chemical Engineering Journal 195–196 (2012) 180–187

Contents lists available at SciVerse ScienceDirect

Chemical Engineering Journal

journal homepage: www.elsevier.com/locate/cej

HKUST-1 MOF: A matrix to synthesize CuO and CuO–CeO_2 nanoparticle catalysts for CO oxidation

Juan M. Zamaro [a,*], Nicolás C. Pérez [a], Eduardo E. Miró [a], Clara Casado [b], Beatriz Seoane [b], Carlos Téllez [b], Joaquín Coronas [b]

[a] Instituto de Investigaciones en Catálisis y Petroquímica, INCAPE (FIQ, UNL, CONICET), Santiago del Estero 2829, 3000 Santa Fe, Argentina
[b] Chemical and Environmental Engineering Department and Instituto de Nanociencia de Aragón (INA), Universidad de Zaragoza, 50018 Zaragoza, Spain

HIGHLIGHTS

- CO oxidation using the metal–organic framework HKUST-1 and Ce/HKUST-1.
- Slow segregation of active 5–15 nm CuO particles upon MOF collapse.
- Synthesis of the highly active CuO–Ce_2O nanoparticle catalyst.
- Effective route to immobilize nanoparticles in a monolith reactor.

GRAPHICAL ABSTRACT

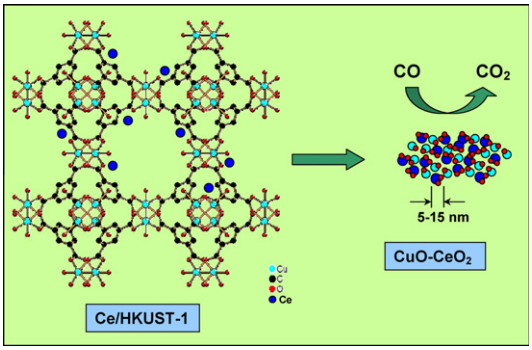

ARTICLE INFO

Article history:
Received 1 March 2012
Received in revised form 23 April 2012
Accepted 25 April 2012
Available online 5 May 2012

Keywords:
Metal–organic framework
$Cu_3(BTC)_2$
Carbon monoxide oxidation
CuO–CeO_2
Nanoparticle synthesis
Monolith

ABSTRACT

The oxidation of carbon monoxide using the metal organic framework (MOF) HKUST-1 is studied. Catalytic results and characterizations by XRD, TEM, H_2-TPR, SEM and LRS show that HKUST-1 itself is not effective in CO oxidation, but is activated in the reaction atmosphere segregating active 5–15 nm CuO particles upon the collapse of the MOF structure. Furthermore, the microporous structure of HKUST-1 is effective to disperse Ce precursors which, upon activation, allow the synthesis of a mixture of CuO and CeO_2 nanoparticles in intimate contact. These nanoparticles present a very high activity in CO oxidation. It is shown that this synthesis route employing HKUST-1 as a matrix is useful to immobilize CuO–Ce_2O nanoparticles in a monolithic reactor, while keeping a high catalytic activity.

1. Introduction

Metal–organic frameworks (MOFs) are a relatively new class of microporous and crystalline materials that consist of inorganic clusters bridged by organic moieties in tridimensional arrangements [1]. They have a high pore volume and some of them have the highest specific surface areas reported to date [2]. These qualities provide MOFs with great potential in applications such as gas capture and storage [3,4], drug release [5], gas separations with membranes [6,7] or by vacuum swing adsorption [8], sensors [9] and heterogeneous catalysis [10,11]. Recently, an extensive revision of the catalytic applications of MOFs has been compiled [12], in which it becomes evident that they have been studied mainly for liquid phase reactions, probably due to the low temperatures involved.

* Corresponding author.
E-mail address: zamaro@fiq.unl.edu.ar (J.M. Zamaro).

1385-8947/$ - see front matter © 2012 Elsevier B.V. All rights reserved.
http://dx.doi.org/10.1016/j.cej.2012.04.091

In general, MOFs have a lower thermal stability than conventional inorganic catalysts. In particular, the metal organic framework HKUST-1 has been used in several liquid phase reactions [13–20]. In contrast, only a few studies have investigated the use of MOFs for heterogeneous gas phase reactions and all of them have focused on CO oxidation which is a reaction that can occur at moderate temperatures. The MOFs studied in this reaction were: a MOF with high thermal stability as ZIF-8 ($[Zn(MeIm)_2 \cdot (DMF)_{0.75}(H_2O)_{1.5}]$) incorporating Au particles [21], a MOF built up by nickel and 4,5-imidazoledicarboxylate (4,5-idc) with an additional alkali metal cation consisting of either Na^+ or Li^+ [22], and a copper-based MOF composed of 5-methylisophthalate ligands $[Cu(mipt)(H_2O)](H_2O)_2$ [23]. Furthermore, Pd/modified MOF-5 was also applied in the oxidation of CO reaching about 90% of conversion at 230 °C [24].

The CO oxidation reaction presents environmental interest because CO is extremely toxic being necessary to be removed from indoor air [25] and also from the H_2 stream used to feed fuel cells that tolerate only a few ppm of CO [26]. Many catalytic formulations have been tested for this reaction and those composed by supported Cu oxides [27], CuO phases dispersed onto CeO_2 [28,29] and $Ce_{1-x}Cu_xO_2$ bimetal oxide nanocomposite catalyst [30] are some of the most promising alternatives. These catalysts avoid the use of noble metals such as Pt and Au [31,32], for which there are limited sources and involve much higher costs while having similar catalytic performance [33]. This scenario suggests, in principle, that a copper-containing MOF could be an advantageous alternative compared to purely inorganic counterparts, in view to the high specific surface areas and low densities of these materials. The MOF $Cu_3(BTC)_2(H_2O)_3 \cdot xH_2O$ (where BTC = benzene 1,3,5-tricarboxylate), denominated HKUST-1, was originally synthesized by Chui et al. in 1999 [34]. It has a high specific surface area (1925 m^2/g) [6] and an interconnected 3D pore system with pore sizes of 9 Å × 9 Å. In addition, HKUST-1 is made of binuclear copper centers that interact weakly with water ligands that can be removed, leaving the metal atoms exposed. It has recently been claimed that this MOF was highly active for CO oxidation, quickly reaching 100% conversion at 240 °C [35]. However, characterization data of the used catalyst were not included despite the fact that this temperature is on the edge of the thermal stability of HKUST-1 [20].

The objective of this work is to study the catalytic performance of HKUST-1 in CO oxidation and to show that this MOF is not active by itself, but that in the reaction stream it has the ability to produce highly dispersed and active CuO nanoparticles. This behavior and the microporous nature of the MOF can be exploited to further synthesize a mixed $CuO–CeO_2$ nanoparticle catalyst highly active in CO oxidation. Moreover, this route of synthesis gives an effective alternative to immobilize nanoparticles in a monolithic structure while preserving high catalytic activity.

2. Experimental

HKUST-1 (Basolite® C-300 from Sigma–Aldrich) was used as received as catalytic material. The solids were evaluated in a continuous flow system equipped with flow mass controllers (MKS). The composition of the reaction flow was 1% CO, 2–20% O_2 in He balance. The reaction was carried out in a glass tubular reactor heated by a furnace with temperature controller at temperatures between 75 °C and 350 °C with flow/mass ratio (F/W) of 330 mL (STP) $min^{-1}g^{-1}$ (typically 60 mg of HKUST-1 and a total flow of 20 mL (STP) min^{-1} were used). In the case of the washcoated monoliths they were placed inside a tubular reactor and the free space between the monolith and the reactor was filled with quartz particles to avoid bypass flow. Prior to the evaluation, the samples were dried in situ under He flow at 120 °C and after that the reaction mixture was fed. The analyses of the gases were performed with a Shimadzu GC-2014 chromatograph equipped with a TCD detector and a column of zeolite 5A. CO conversions (X_{CO}) were calculated as: $X_{CO} = \frac{[CO]^\circ - [CO]}{[CO]^\circ}$; where X is conversion, $[CO]^\circ$ and [CO] are inlet and outlet gas concentrations in ppm, respectively.

To obtain the catalysts with Ce, HKUST-1 samples were impregnated with a 1 M ethanolic solution of Ce(III) nitrate hexahidrate (Sigma–Aldrich, 99%). The incipient wetness impregnations were performed in order to get mass ratios of Cu/Ce = 1, 0.5 and 0.3 in the solids. The catalysts were dried at 60 °C overnight. Furthermore, HKUST-1 and Ce-HKUST-1 coatings on cordierite honeycomb monoliths (Corning, 400 cps, 0.17 mm average wall thickness) were obtained. The monoliths containing 64 channels (1 cm × 1 cm of section and 2 cm long) were washcoated with ethanolic suspensions of 10 wt.% of HKUST-1. The procedure was similar to that employed with zeolites [36]. For Ce containing sample, a washcoated HKUST-1 monolith was later impregnated with a $Ce(NO_3)_3$ ethanolic solution.

Characterizations were performed by X-ray diffraction (XRD) with a Shimadzu XD-D1 instrument at an acquisition rate of $2°min^{-1}$ between $2\theta = 5°$ a 55° employing a Cu Kα radiation with $\lambda = 1.5418$ Å at 30 kV and 40 mA. Scanning electron microscopy (SEM) was performed with a JEOL JSM-35C instrument, operated at 20 kV acceleration voltages. Temperature-programmed reduction with hydrogen (H_2-TPR) was performed in an Okhura TP-2002S equipped with a TCD detector. The sample was first pretreated in situ with N_2 for 1 h at 200 °C before the TPR. After that, it was cooled at r.t. in N_2 flow and the TPR was immediately run in a 5% H_2–Ar stream (15 mL(STP) min^{-1}), at 10 °C min^{-1}. Thermogravimetric analyses (TGA) were performed in a Mettler Toledo STARe with a TGA/SDTA851e module from 25 °C to 400 °C at of 10 °C min^{-1} in a flow of air. Transmission electron microscopy (TEM) analyses were performed in a JEOL 2000 FXII and in a TECNAI T20 instruments. HAADF–STEM (high angle angular dark-field scanning transmission microscopy) analyses were performed in a TECNAI F30 TEM–STEM microscope. The samples were dispersed in ethanol in an ultrasound bath for 15 min and then poured on carbon–copper grids prior to observation. Laser Raman spectroscopy (LRS) was performed using a LabRam spectrometer (Horiba-Jobin-Yvon) coupled to an Olympus confocal microscope equipped with a CCD detector cooled to about 200 K. The excitation wavelength was 532 nm (Spectra Physics argon-ion laser). The laser power was set at 30 mW.

3. Results and discussion

3.1. CO oxidation on HKUST-1 with different pretreatments

Table 1 summarizes the characteristics and treatments of all samples tested in this work. Fig. 1 shows the CO conversion curves of HKUST-1 (HK1) obtained with increasing temperatures, where measurements were performed 15 min after reaching the desired temperature. A sharp increase can be observed in the conversion level, presenting 26% of conversion after 80 min at 230 °C, whereas the conversion reached 69% after another 90 min at 240 °C. So far, the behavior was similar to that recently reported in the literature [35].

Subsequently, the sample was brought to 300 °C and maintained in reaction atmosphere for 30 min, and then conversions at progressively decreasing temperatures were measured. As shown in Fig. 1, a large increase in the activity of the material was observed (HK2), shifting the conversion curve toward lower temperatures. Whereas another sample of HKUST-1 was pretreated in flowing air at 400 °C for 1 h and the resulting solid

Table 1
Treatments and characteristics of all the evaluated catalysts.

Sample Id	Crystallite size (nm)[a]	T^{50} (°C)[b]	Treatment[c]
HK1	–	235	A
HK2	11.6	175	A + S
HK3	19.7	–	P
HK4-82	–	–	I1
HK4-100	5.3	143	I2 + S
HK5-2	–	210	A + S + C
HK5-20	15.4	200	A + S + C + O
HKCe(1)		137	A + S
HKCe(0.3)	5.6 (CeO_2)	135	A + S
HKCe(0.5)		111	A + S
HKCe(0.5b)		113	A + S
HK/monolith	–	171	A + S
HKCe/monolith	–	124	A + S

A: activation produced in reaction atmosphere during the first catalytic run of fresh HKUST-1.
S: stabilizing treatment after activation, for 30 min at 300 °C.
P: pyrolysis in air up to 400 °C.
C: cyclic evaluations in runs with increasing and decreasing temperatures.
O: evaluation performed with a 20% of O_2.
I1: isothermal treatment at 240 °C in reaction atmosphere during 264 min until the sample reached 82% conversion.
I2: isothermal treatment at 240 °C in reaction atmosphere during 324 min until the sample reached 100% conversion.
[a] Calculated by Scherrer's equation.
[b] Temperature at which 50% conversion was reached.
[c] Treatment applied at each sample.

showed very low activity (HK3). This suggests that in the reaction stream containing diluted CO and O_2 the MOF underwent a strong activation, probably by some change in their physicochemical characteristics. Hereafter, we refer to as activation of fresh HKUST-1 the treatment in the first catalytic run and as stabilization the maintenance of this activated sample for 30 min at 300 °C.

During the first catalytic run an unstable behavior of the conversions was observed at temperatures close to 230 °C, i.e. keeping the solid at that temperature for a few minutes did not stabilize their activity level. To gain further insight, a new HKUST-1 sample was heated in reaction atmosphere at 5 °C min^{-1} to 240 °C and maintained at this temperature. Fig. 2 shows that the activity evolved from zero to 82% conversion in approximately 4 h (HK4-82) and reached 100% conversion in approximately 5.5 h (HK4-100). The conversion reached by the HK4-82 sample is

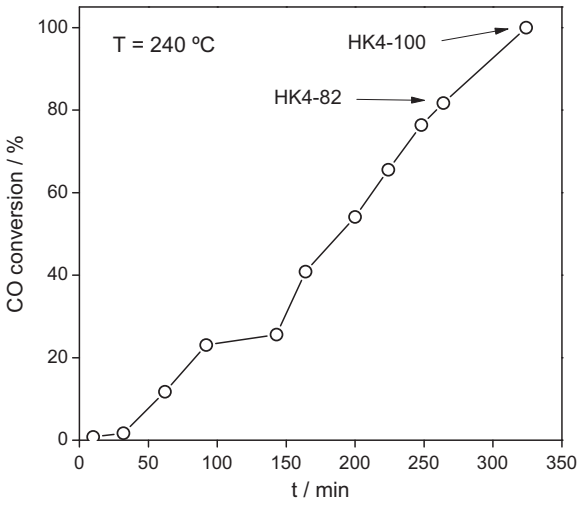

Fig. 2. Evolution of CO conversion with HKUST-1 maintained isothermally at 240 °C in reaction atmosphere.

comparable to that of sample HK1 (Fig. 1) which remained at 230–240 °C for 170 min. This sample was stabilized for 30 min at 300 °C and the measured activity was even greater than in the previous cases as shown in Fig. 3. It should be noted that in our TG analysis in air (not shown) HKUST-1 showed very small mass loss up to 300 °C, while Schlichte et al. [20] observed by high-temperature XRD that HKUST-1 kept in Ar atmosphere, start to decompose at 260 °C generating Cu^0 particles with a loss of the MOF crystallinity. On the other hand, in the pioneering work by Chui et al. [34], it was found by TGA (in N_2) and high-temperature single-crystal X-ray diffractometry that HKUST-1 was stable only up to 240 °C.

Another fresh sample (HK5) was activated and stabilized and then maintained at 200 °C for 9 h. After that, activity was measured in cycles of increasing and decreasing temperature. A slight hysteresis is observed among the conversion points, which is a common feature for the CO oxidation reaction. The constancy in the position of the hysteresis indicates that is provoked by a catalytic effect, explained by differences in CO and O_2 coverage upon heating and cooling [37] and not by a physicochemical change in the catalyst.

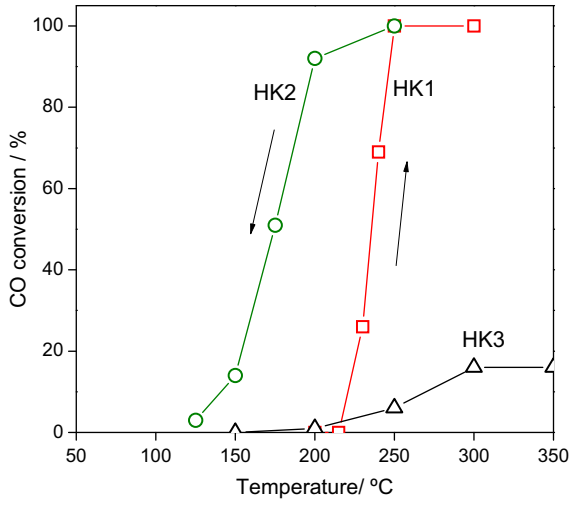

Fig. 1. Catalytic CO oxidation curves. HK1: HKUST-1 evaluated in increasing temperatures; HK2: solid evaluated in decreasing temperatures after being kept HK1 at 300 °C for 30 min; HK3: curve of HKUST-1 calcined in air at 400 °C.

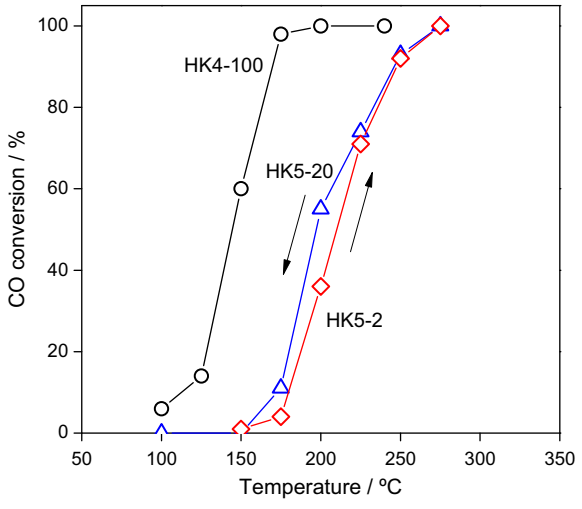

Fig. 3. Catalytic curves of activated HKUST-1. Sample isothermally activated (HK4-100). Activated sample evaluated with 2% O_2 and 20% O_2 (HK5-2 and HK5-20, respectively).

This means that the catalyst was stable during the evaluation period; even though the activity was lower now than for the HK2 solid. In fact the CO conversion at 200 °C after 36 h of time-on-stream passed from 42% to 39%. Fig. 3 presents the first evaluation curve during a heating run with 2% oxygen (HK5-2) and a final evaluation of the same sample increasing by 20% the oxygen concentration in the reaction flow (HK5-20). It can be seen that conversion values were approximately the same, which indicates a zero order reaction with respect to O_2. This behavior coincides with that shown by catalysts based on supported CuO particles [38].

3.2. Characterization of fresh and used HKUST-1 catalysts

Fig. 4 shows the XRD patterns of the solids previously evaluated. In general, all samples showed diffraction signals corresponding to CuO and some of them also showed small peaks of Cu_2O. Fresh HKUST-1 presented all the previously indexed diffraction signals for this material [34]. In contrast, the MOF structure collapsed for HK2 and three signals appeared at $2\theta = 35.3°$, 38.5° and 48.6°, which correspond to the main reflections of CuO (JCPDS 44–706) and a small signal (36.5°) from the main reflection of Cu_2O (ICDD 5–667) was also observed. The experimental XRD pattern of bulk CuO is also presented, where it is worth noting that the main signals of CuO are located very close to some of HKUST-1 ($2\theta = 35.1°$, 38.9°). In any event, this confirms that the activity of HK2 is due to CuO particles generated by decomposition of the HKUST-1 and not by the Cu present in the crystal lattice of the MOF. Moreover, the XRD signals of this sample are broad, indicating a small crystal size that explains the high activity observed. Meanwhile, in the diffractogram of HK3 sample there are also signals of CuO, but sharper than in HK2. The crystallite sizes were calculated using the Scherrer's equation, being for samples HK2 and HK3 $t_{HK2} = 11.6$ nm and $t_{HK3} = 19.7$ nm, respectively. The formation of highly crystalline CuO in the HK3 sample was similar to that reported from HKUST-1 pyrolyzed at 600 °C in air atmosphere [39]. An H_2-TPR of the HK3 sample showed a reduction signal that initiated at 270 °C. Then, the low activity of this solid may be mainly ascribed to its larger crystallite size.

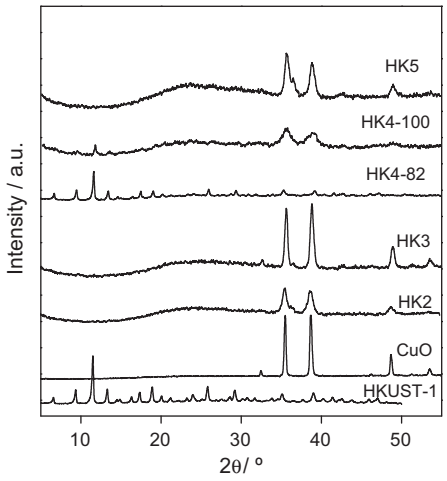

Fig. 4. XRD patterns of as received HKUST-1, bulk CuO and the activated samples HK2, HK3, HK4 and HK5-20.

The XRD of HKUST-1 evaluated at 240 °C that reached 82% conversion (HK4-82) showed a loss of MOF crystallinity given the lower intensity of all reflections. Crystallinity can be estimated as 40% considering the area under the main peaks ($2\theta = 9.4°$, 11.5°, 13.3° and 17.4°) and taking 100% for fresh HKUST-1 as reference. It is difficult to distinguish the signals of CuO in this sample because it was taken for XRD measurement during the activation process and only a relatively low amount of Cu would have segregated outside the MOF. This sample was placed again in reaction at 240 °C and allowed to evolve until reaching 100% conversion (HK4-100). After that, HKUST-1 signals virtually disappeared (Fig. 4) remaining only a signal at $2\theta = 11.5°$ (HKUST-1 crystallinity 5%) while broad CuO signals arose having Scherreŕs $t_{HK4} = 5.4$ nm. The small nanoparticle size was responsible for the high activity of this sample, whereas the crystal size for the HK5 sample was $t_{HK5} = 15.3$ nm, in agreement with the slightly lower activity of this sample with respect to that of HK2 (Table 1).

The TEM image of collapsed HKUST-1 (Fig. 5a) showed dispersed nanoparticles having a cluster-like aspect, with an average single particle size of about 10 ± 4 nm in agreement with XRD findings. From the analysis of the selected area electron diffraction (SAED) pattern (Fig. 5b and c), it was possible to determine that these nanoparticles correspond to crystalline CuO as shown by

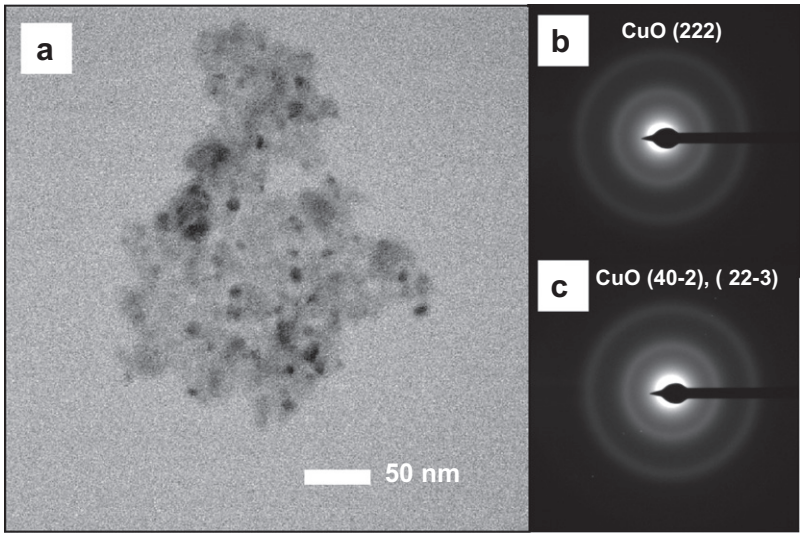

Fig. 5. (a) TEM image showing dispersed nanoparticles in sample HK4; (b) SAED patterns taken in a sector of the same sample, showing that nanoparticles correspond to pure CuO. The diffractions are from (222), (40–2) and (22–3) planes.

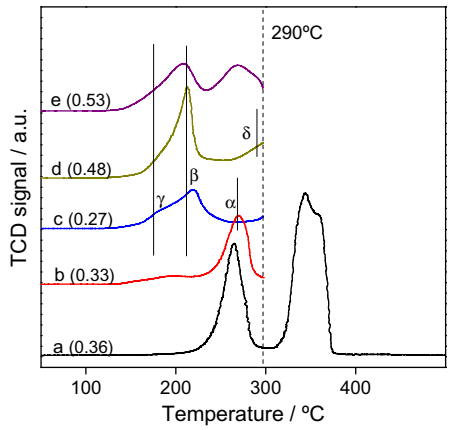

Fig. 6. (a) H_2-TPR profile of HKUST-1. (b–e) Successive H_2-TPR profiles of HKUST-1 performed until 290 °C with intermediate oxidations in air flow at 200 °C. The H_2 consumption up to 290 °C (μmol H_2/μmol Cu) is given between brackets.

the intense diffraction patterns with 0.112 nm and 1.113 nm lattice spacing that can be indexed as the (222) and (40–2), (22–3) planes of this oxide [40,41], respectively.

Fig. 6a shows the H_2-TPR profile of HKUST-1 in which H_2 consumption starts at about 200 °C (maximum at 265 °C) and another after 300 °C. The first one may be assigned to the reduction of Cu(II) of the HKUST-1, showing their instability in a diluted stream of H_2 at temperatures slightly above 200 °C. The reduction temperature of this copper is lower compared to that of bulk CuO, which usually starts reducing at temperature $\geqslant$300 °C [42]. Since HKUST-1 decomposes with mass loss at temperatures above 300 °C, the second H_2-TPR signal can be assigned to the evolution of the decomposition gases, recorded by TCD and to CuO produced by the thermal decomposition of the MOF. When another H_2-TPR of a fresh HKUST-1 sample was run up to 290 °C (Fig. 6b), the first peak due to the reduction of Cu(II) from the MOF network was again observed (α). When in situ oxidation up to 290 °C with air stream followed by H_2-TPR was performed, new signals appeared centered at 180 °C (γ) and 210 °C (β), which can be attributed to highly dispersed CuO species generated by the oxidation of (α) species that disappeared. These dispersed CuO had a similar behavior to that found for supported small CuO particles [43]. From the H_2 consumption up to 290 °C (indicated as μmol H_2/μmol Cu in Fig. 6) and considering the stoichiometry, it can be inferred that not all the Cu present in MOF was reduced up to 290 °C. After several cycles of oxidation followed by TPR, another signal (δ) appeared at higher temperatures (Fig. 6c–e). In view of the increased consumption in the latter cycles, this signal would be a product of larger CuO particles generated by a progressive thermal decomposition of the MOF at temperatures above 240 °C during the redox sequence. It is noteworthy that in all patterns very small particles were detected because they started reducing at temperatures as low as 130 °C, revealing the ability of HKUST-1 to generate dispersed CuO nanoparticles.

The SEM images of as received HKUST-1 (Fig. 7a and b) show polyhedral crystals presenting well-defined edges and crystal facets with a size of 12.4 ± 3.7 μm. In contrast, the degraded sample (Figs. 7c and d) shows a shapeless, fold appearance. This morphology is similar to that of the so-called coralloid Cu 3D observed for CuO produced after the thermolysis of HKUST-1 [44]. The generation of Co_3O_4 particles, which were active in the oxidation of CO, both by decomposition of the MOF ZIF-67 and Co-ZIF-8 has been recently reported [45].

The above results show that the atomic and periodic dispersion of Cu in the tridimensional framework of HKUST-1 turns it into a useful matrix to obtain finely and homogeneously dispersed active CuO nanoparticles.

3.3. Catalytic behavior and characterizations of Ce/HKUST-1 catalysts

Taking into account the ability of HKUST-1 to generate dispersed CuO, the porous net of this MOF could also be used as a temporary host to accommodate precursors of other oxides before the degradation of the network during the activation process. Since

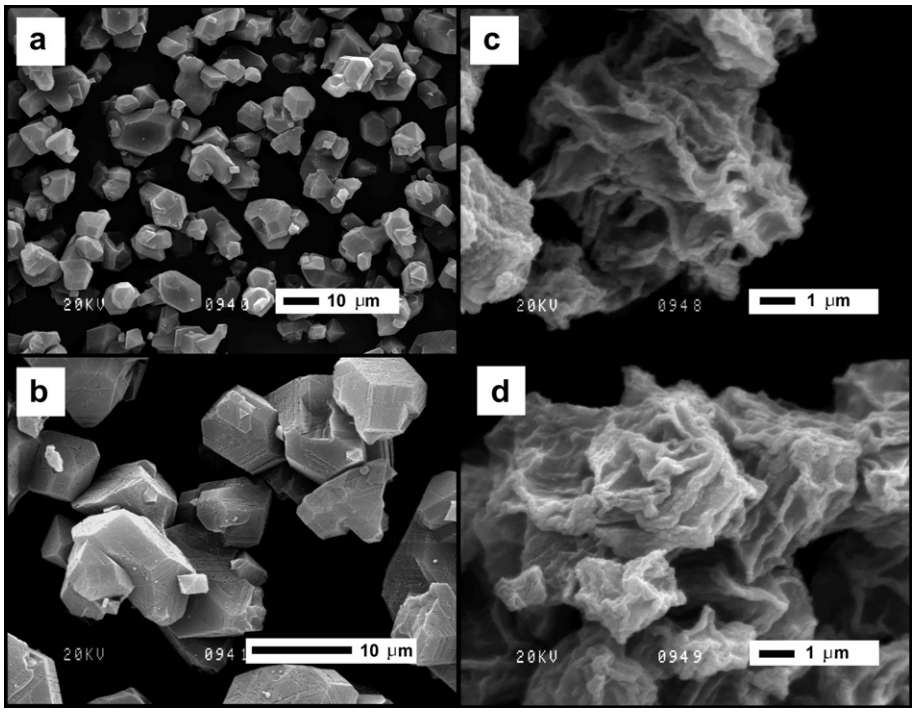

Fig. 7. (a and b) SEM images of as received HKUST-1 crystals; (c and d) SEM images of activated HKUST-1.

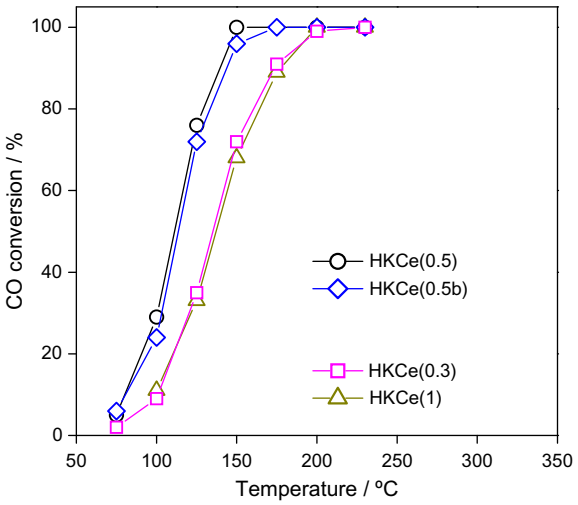

Fig. 8. CO oxidation curves of samples HKCe(1); HKCe(0.5); HKCe(0.5b) and HKCe(0.3), containing Cu/Ce mass ratios of 1, 0.5, 0.5 and 0.3, respectively.

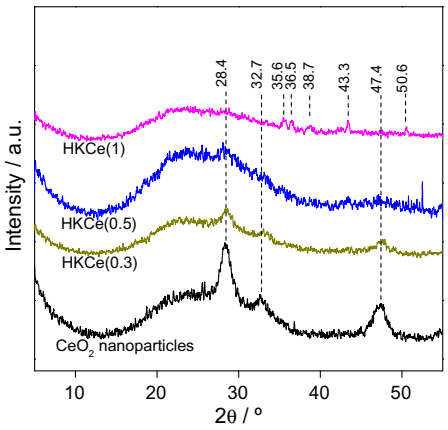

Fig. 9. XRD patterns of Cu–Ce containing samples derived from activation of Ce/HKUST-1. Pattern of CeO_2 nanoparticles (10–20 nm) were obtained from Nyacol.

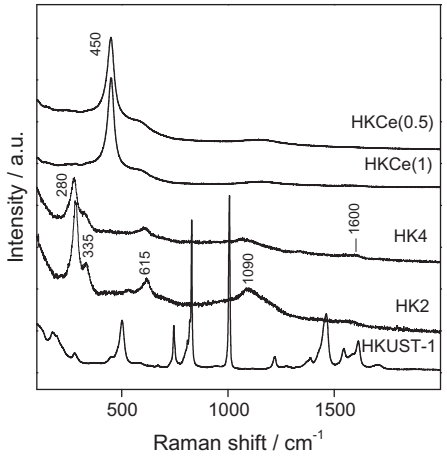

Fig. 10. LRS spectra of HKUST-1, activated HKUST-1 and activated Ce/HKUST-1 samples.

$Ce(NO_3)_3$ is fully decomposed before 280 °C to form CeO_2 (TGA not shown), this salt can be used to generate this oxide simultaneously to the CuO from the HKUST-1 above 300 °C. Under this assumption, HKUST-1 was impregnated with ethanolic solutions of $Ce(NO_3)_3$ containing different Cu/Ce mass ratios (Section 2). By treating these solids in reaction conditions after the initial pretreatments a fast activation around 215–230 °C was observed, rapidly reaching 100% conversion. All the Ce modified HKUST-1 samples are presented in Table 1.

The Ce modified HKUST-1 samples were activated and stabilized and then catalytically evaluated measuring conversion towards lower temperatures (Fig. 8). A significant increase in activity compared with the samples without Ce was observed. Samples HKCe(1) and HKCe(0.3) showed a somewhat lower activity than of HKCe(0.5), indicating an optimal Cu/Ce proportion. In view of these results, another sample with a Cu/Ce ratio of 0.5 was prepared (HKCe(0.5b)) and the activity of this sample was very similar to that of HKCe(0.5), showing the reproducibility of the preparation method. The existence of optimal proportions of CuO–CeO_2 in catalysts for CO oxidation has already been reported for CuO–promoted CeO_2 catalysts [46], while the activity improvement in this reaction is provided by a synergism developed between both oxide particles at their interphase [47]. In comparison to other Cu–Ce based catalysts, the activity of the catalyst derived from HKUST-1 was high (T^{50} = 111 °C, and complete conversion below 150 °C), which is similar to the best CuO–CeO_2 catalysts synthesized by other conventional techniques [28–30]. However, this comparison is approximate because the W/F ratios were different.

As shown in Fig. 9 the HKCe(0.3) and HKCe(0.5) catalysts present XRD signals of cubic fluorite type CeO_2 phase with reflections at 2θ = 28.4°, 32.7° and 47.4° (ICDD 34–0394), which can also be compared with the experimental pattern of crystalline CeO_2 nanoparticles. In general, the low intensity of the reflections is probably due both to the small amount of sample available for analysis and their low crystallinity. From reflection of (1 1 1) plane (2θ = 28.4°), crystallite size of CeO_2 was calculated in 5.6 nm. In addition, the reflections of CuO (35.6°; 38.7°) and Cu_2O (36.5°) can be distinguished in the HKCe(1) sample. It was possible to gain further information of these samples by Laser Raman spectroscopy (LRS). Fig. 10 shows common LRS bands for HKUST-1 [48], the most intense being located at 500 cm^{-1} related to vibrational modes directly involving Cu(II) species, 745 and 829 cm^{-1} ascribed to out-of-plane ring (C–H) bending vibrations and 1006 cm^{-1} (associated with C=C modes of the benzene ring). When HKUST-1 was activated, all MOF signals disappeared in line with the collapse of their framework. Simultaneously, there appeared the bands located at 280, 335 and 615 cm^{-1} and a broad peak near 1090 cm^{-1}, as shown in the spectra for the HK2 and HK4 materials. All these signals correspond to CuO [43], which is consistent with XRD, TEM and SAED observations. Additionally, a weak signal was observed at 1600 cm^{-1} which is characteristic of graphite, probably from small amounts of carbonaceous residues coming from the HKUST-1 degradation. In activated Ce/HKUST-1 samples, CuO LRS signals were also observed as well as a strong signal at 450 cm^{-1}, which is due to CeO_2 [43,49]. The slight shift of this band to a lower frequency is an evidence of the small crystal size of CeO_2 [49]. The TEM image of Fig. 11a also shows small particles of about 5 nm that are attributed to CeO_2, in agreement with the previously calculated Scherreŕs size. Moreover, as shown in Fig. 11b, the SAED diffraction patterns halos obtained from these catalysts, show a lattice spacing of 0.122(4) nm that can be indexed as the (3 3 1) crystalline planes of CeO_2. Besides, a diffraction halo with a 0.231 nm spacing indexed as the (2 0 0) CuO plane is observed.

An HAADF image of HKCe(1) sample is shown in Fig. 12a. The contrast in this type of image depends both on the thickness of the sample and the atomic number of the elements, therefore, containing chemical information. The heavier Ce particles appeared

brighter than Cu and it can be observed that the copper and cerium atoms are closely packed. Fig. 12b and c shows the EDS spectra taken from the areas indicated as 1 and 2, respectively. The coexistence of X-ray signals of Cu and Ce coming from the small selected analysis area confirms the close contact between both oxides.

The incorporation of Ce in HKUST-1 allows obtaining highly dispersed phases of CuO and CeO_2 in high interaction which gives a highly active nanoparticulated catalyst.

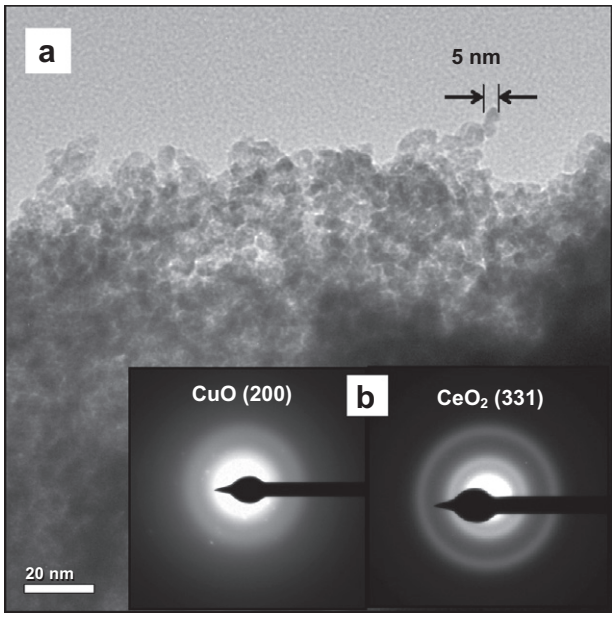

Fig. 11. (a) TEM image of HKCe(0.5) sample; (b) SAED patterns of the same sample, showing the diffraction of the (200) plane of CuO and the (331) plane of CeO_2.

3.4. Immobilization of CuO–CeO_2 nanoparticles in a monolith reactor

The synthesis of the CuO–CeO_2 from HKUST-1 is an attractive route to immobilize the catalytic nanoparticles in a monolithic reactor. Since the MOF crystals have a size compatible with the pore size of the walls of cordierite monoliths (10–50 μm), they could be anchored and subsequently activated generating the immobilized nanoparticles. The coating from a slurry, commonly called washcoating, is usually carried out with a slurry of particles of a comparable size to that of the macropores of the support [50]. To this end, cordierite monoliths were washcoated with HKUST-1 (HK/monolith) and Ce/HKUST-1 (HKCe/monolith). The MOF crystals were able to be firmly retained in the monolith walls and were well distributed throughout the length of the channels although without completely covering the substrate, as shown in Fig. 13a. In view of the proper anchorage of the crystals, HUKST-1 and Ce-HKUST-1 monoliths were then activated and stabilized in the reaction atmosphere. As shown in Fig. 13b, the performance of both monoliths (evaluated under the same conditions as the other catalysts) was very similar to that of the respective powders, being T^{50} = 171 °C and T^{50} = 124 °C for the HK/monolith and the HKCe/monolith, respectively.

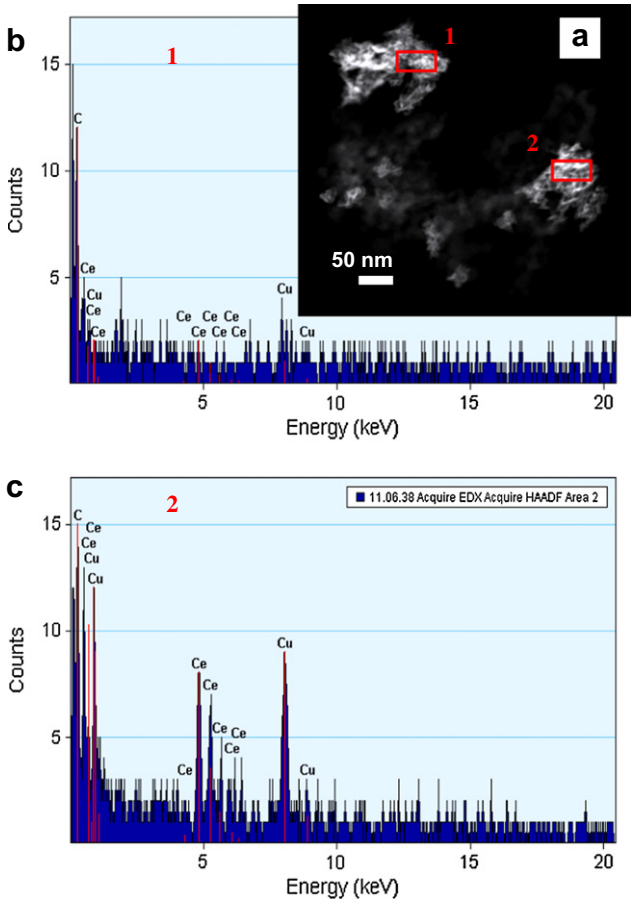

Fig. 12. (a) HAADF image of HKCe(0.5) sample; (b and c) EDS spectra collected from the selected areas 1 and 2, respectively.

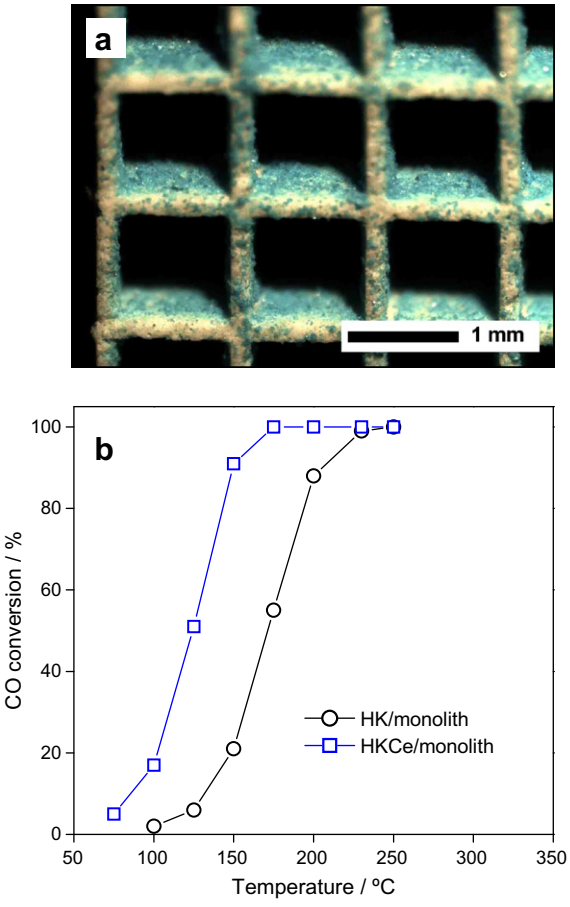

Fig. 13. (a) Microscope image of HKUST-1/monolith after washcoat; (b) CO oxidation curves for activated HKUST-1/monolith and Ce-HKUST-1/monolith.

4. Conclusions

MOF HKUST-1 proved to be ineffective in the oxidation of CO; what resulted active was its transformation product generated in the reaction atmosphere at temperatures above 230 °C. This transformation involves a gradual segregation of CuO nanoparticles from the MOF, simultaneously with a loss of MOF crystallinity. The incorporation of a Ce precursor in the network of HKUST-1 with a subsequent activation yielded a highly dispersed mixture of CuO and CeO_2 nanoparticles with a high degree of interaction that is highly active in CO oxidation. Finally, it has been shown that the anchoring and subsequent activation of the HKUST-1 and Ce-HKUST-1 coatings is a novel and effective route for synthesizing immobilized CeO_2–CuO nanoparticles in a monolithic reactor, thus preserving their high catalytic activity.

Acknowledgements

The financial support of CONICET and ANPCyT from the Argentine government and from Universidad Nacional del Litoral is acknowledged. Universidad de Zaragoza gratefully acknowledges financial support from the Spanish Ministry of Science and Innovation (MAT2010-15870 and FPU Program). The authors are also grateful to the Laboratorio de Microscopías Avanzadas at the Instituto de Nanociencia de Aragón of the Universidad de Zaragoza and to Prof. E. Grimaldi for the English language editing.

References

[1] J.L.C. Rowsell, O.M. Yagui, Micropor. Mesopor. Mater. 73 (1–2) (2004) 3–14.
[2] G. Férey, Chem. Soc. Rev. 37 (1) (2008) 191–214.
[3] C. Chen, J. Kim, D.A. Yang, W.S. Ahn, Chem. Eng. J. 168 (2011) 1134–1139.
[4] C.M. Lu, J. Liu, K. Xiao, A.T. Harris, Chem. Eng. J. 156 (2010) 465–470.
[5] P. Horcajada, C. Serre, M. Vallet-Regi, M. Sebban, F. Taulelle, G. Férey, Angew, Chem. Int. Ed. 45 (2006) 5974–5978.
[6] B. Zornoza, B. Seoane, J.M. Zamaro, C. Téllez, J. Coronas, Chem. Phys. Chem. 12 (15) (2011) 2781–2785.
[7] H. Bux, F.Y. Liang, Y.S. Li, J. Cravillon, M. Wiebcke, J. Caro, J. Am. Chem. Soc. 131 (2009) 16000–16001.
[8] A.F.P. Ferreira, J.C. Santos, M.G. Plaza, N. Lamia, J.M. Loureiro, A.E. Rodrigues, Chem. Eng. J. 167 (2011) 1–12.
[9] Y. Takashima, V.M. Martinez, S. Furukawa, M. Kondo, S. Shimomura, H. Uehara, M. Nakahama, K. Sugimoto, S. Kitagawa, Nat. Commun. 2 (2011) 168–175.
[10] S. Naito, T. Tanibe, E. Saito, T. Miyao, W. Mori, Chem. Lett. (2001) 1178–1179.
[11] J. Gascon, U. Aktay, M.D. Hernandez-Alonso, G.P.M. van Klink, F. Kapteijn, J. Catal. 261 (2009) 75.
[12] A. Corma, H. García, F.X. Llabrés i Xamena, Chem. Rev. 110 (2010) 4606–4655.
[13] A. Dhakshinamoorthy, M. Alvaro, H. Garcia, ACS Catal. 1 (2011) 48–53.
[14] A. Dhakshinamoorthy, M. Alvaro, H. Garcia, J. Catal. 267 (2009) 1–4.
[15] I. Luz, F.X. Llabrés i Xamena, A. Corma, J. Catal. 276 (2010) 134–140.
[16] L. Kurfirtová, Y.-K. Seo, Y.K. Hwang, J.-S. Chang, J. Cejkaa, Catal. Today 179 (2012) 85–90.
[17] N.B. Pathan, A.M. Rahatgaonkar, Mukund S. Chorghade, Catal. Commun. 12 (2011) 1170–1176.
[18] E. Pérez-Mayoral, J. Čejka, Chem Cat Chem 3 (1) (2011) 157–159.
[19] L.H. Wee, N. Janssens, S.R. Bajpe, C.E.A. Kirschhock, J.A. Martens, Catal. Today 171 (2011) 275–280.
[20] K. Schlichte, T. Kratzke, S. Kaskel, Micropor. Mesopor. Mater. 73 (2004) 81–88.
[21] H.-L. Jiang, B. Liu, T. Akita, M. Haruta, H. Sakurai, Q. Xu, J. Am. Chem. Soc. 131 (2009) 11302–11303.
[22] R.Q. Zou, H. Sakurai, Q. Xu, Angew, Chem., Int. Ed. 45 (2006) 2542–2546.
[23] R.Q. Zou, H. Sakurai, S. Han, R.Q. Zhong, Q. Xu, J. Am. Chem. Soc. 129 (2007) 8402–8403.
[24] W. Kleist, M. Maciejewski, A. Baiker, Thermochim. Acta 499 (2010) 71–78.
[25] E. Green, S. Short, IEH Assessment on Indoor Air Quality in the Home (2): Carbon Monoxide, Leicester, 1998.
[26] H. Igarashi, T. Fujino, M. Watanabe, J. Electroanal. Chem. 391 (1995) 119–123.
[27] P. Doggali, S. Waghmare, S. Rayalu, Y. Teraoka, N. Labhsetwar, J. Mol. Catal. A: Chem. 347 (2011) 52–59.
[28] X. Zheng, S. Wang, S. Wang, S. Zhang, W. Huang, S. Wu, Catal. Commun. 5 (2004) 729–732.
[29] K.N. Rao, P. Bharali, G. Thrimurthulu, B.M. Reddy, Catal. Commun. 11 (2010) 863–866.
[30] H. Mai, D. Zhang, L. Shi, T. Yan, H. Li, Appl. Surf. Sci. 257 (2011) 7551–7559.
[31] J.L. Ayastuy, M.P. González-Marcos, J.R. González-Velasco, M.A. Gutiérrez-Ortiz, Appl. Catal. B 70 (2007) 532–541.
[32] C. Galletti, S. Fiorot, S. Specchia, G. Saracco, V. Specchia, Chem. Eng. J. 134 (2007) 45–50.
[33] A. Razegui, A. Khodadadi, H. Ziaei-Azad, Y. Mortazavi, Chem. Eng. J. 164 (2010) 214–220.
[34] S.S.-Y. Chui, S.M.-F. Lo, J.P.H. Charmant, A.G. Orpen, I.D. Williams, Science 283 (1999) 1148–1150.
[35] J-y. Ye, C-j. Liu, Chem. Commun. 47 (2011) 2167–2169.
[36] J.M. Zamaro, M.A. Ulla, E.E. Miró, Chem. Eng. J. 106 (2005) 25–33.
[37] M. Lepage, T. Visser, F. Soulimani, A.M. Beale, A. Iglesias-Juez, Ad.M.J. van der Eerden, B.M. Weckhuysen, J. Phys. Chem. C 112 (2008) 9394–9404.
[38] E. Miró, E. Lombardo, J. Petunchi, J. Catal. 104 (1) (1987) 176–185.
[39] L. Chen, C. Zhao, Z. Wei, S. Wang, Y. Gu, Mater. Lett. 65 (2011) 446–449.
[40] F. Zhang, S.-W. Chan, J.E. Spanier, E. Apak, Q. Jin, R.D. Robinson, I.P. Herman, Appl. Phys. Lett. 80 (2002) 127–129.
[41] S. Turner, O.I. Lebedev, F. Schröder, D. Esken, R.A. Fischer, G.V. Tendeloo, Chem. Mater. 20 (2008) 5622–5627.
[42] J. Xiaoyuan, L. Guanglie, Z. Renxian, M. Jianxin, C. Yu, Z. Xiaoming, Appl. Surf. Sci. 173 (2001) 208–220.
[43] H. Mai, L. Mengfei, F. Ping, J. Rare Earths 24 (2006) 188–192.
[44] L. Chen, Y. Shen, J. Bai, C. Wang, J. Solid State Chem. 182 (2009) 2298–2306.
[45] W. Wang, Y. Li, R. Zhang, D. He, H. Liu, S. Liao, Catal. Commun. 12 (2011) 875–879.
[46] M. Jobbágy, F. Mariño, B. Schonbrod, G. Baronetti, M. Laborde, Chem. Mater. 18 (2006) 1945–1950.
[47] A. Martínez-Arias, D. Gamarra, M. Fernández-García, X.Q. Wang, J.C. Hanson, J.A. Rodriguez, J. Catal. 240 (2006) 1–7.
[48] C. Prestipino, L. Regli, J.G. Vitillo, F. Bonino, A. Damin, C. Lamberti, A. Zecchina, P.L. Solari, K.O. Kongshaug, S. Bordiga, Chem. Mater. 18 (2006) 1337–1346.
[49] S. Wang, W. Wang, J. Zuo, Y. Quian, Mat. Chem. Phys. 68 (2001) 246–248.
[50] T.A. Nijhuis, A.E.W. Beers, T. Vergunst, I. Hoek, F. Kapteijn, J.A. Moulijn, Catal. Rev. 43 (4) (2001) 345–380.